6-9-2011

On the Origin of Fluctuations in the Cusp Diamagnetic Cavity

K. Nykyri
Embry-Riddle Aeronautical University, nykyrik@erau.edu

A. Otto
University of Alaska, Fairbanks

E. Adamson
University of Alaska, Fairbanks

A. Tjulin
EISCAT Scientific Association

On the origin of fluctuations in the cusp diamagnetic cavity

K. Nykyri,[1] A. Otto,[2] E. Adamson,[2] and A. Tjulin[3]

Received 30 June 2010; revised 28 February 2011; accepted 7 March 2011; published 9 June 2011.

[1] We have analyzed Cluster magnetic field and plasma data during high-altitude cusp crossing on 14 February 2003. Cluster encountered a diamagnetic cavity (DMC) during northward interplanetary magnetic field (IMF) conditions, and as IMF rotated southward, the spacecraft reencountered the cavity more at the sunward side. The DMC is characterized by a high level of magnetic field fluctuations and high-energy electrons and protons. Ultralow-frequency turbulence has been suggested as a mechanism to accelerate particles in DMC. We demonstrate in this paper for the first time that many of the low-frequency fluctuations in the cavity are back and forth motion of the DMC boundaries over the spacecraft and transient reconnection signatures. We also find examples of some isolated high-amplitude waves that could possibly be nonlinear kinetic magnetosonic modes. The lack of strong wave power at the vicinity of local ion cyclotron frequency in the DMC suggests that perhaps a mechanism other than wave-particle heating is a dominant source for ion heating in DMCs.

Citation: Nykyri, K., A. Otto, E. Adamson, and A. Tjulin (2011), On the origin of fluctuations in the cusp diamagnetic cavity, *J. Geophys. Res.*, *116*, A06208, doi:10.1029/2010JA015888.

1. Introduction

[2] The magnetosheath plasma has the most direct access to the ionosphere through high-altitude cusps [*Heikkilä and Winningham*, 1971; *Frank and Ackerson*, 1971]. The large-scale cusp structure is determined by the occurrence of magnetic reconnection at the high-latitude magnetopause for northward interplanetary magnetic field (IMF) and at the low-latitude magnetopause for southward IMF [*Lavraud et al.*, 2005a]. The plasma accumulation on newly opened field lines in the vicinity of the cusps leads to the formation of extended regions of high plasma beta and depressed magnetic field [*Lavraud et al.*, 2004]. These so-called diamagnetic cavities (DMCs) often show high fluxes of high-energy particles: electrons, protons, oxygen and helium ions [*Chen and Fritz*, 1998; *Fritz et al.*, 1999; *Chen and Fritz*, 2001; *Zhang et al.*, 2005; *Whitaker et al.*, 2006, 2007; *Walsh et al.*, 2007; *Niehof et al.*, 2008; *Walsh et al.*, 2010] and a high level of magnetic field fluctuations of the order of $dB/B \sim 1$ [*Chen and Fritz*, 1998].

[3] The origin of the high-energy particles in the cavity has been a longstanding and controversial topic. Currently there are three theories on the origin of these high-energy populations: (1) local acceleration [*Chen and Fritz*, 1998; *Chen*, 2008], (2) bow shock source [*Chang et al.*, 1998; *Trattner et al.*, 1999; *Chang et al.*, 2000; *Trattner et al.*, 2001], and (3) magnetospheric source [*Kremser et al.*, 1995; *Delcourt and Sauvaud*, 1998, 1999; *Blake*, 1999; *Lavraud et al.*, 2005b; *Asikainen and Mursula*, 2005, 2006].

[4] Understanding the origin and nature of these magnetic field fluctuations in DMCs is important as particles may potentially gain energy from wave-particle interactions. It has been argued that the ultralow-frequency "turbulence" in the DMCs can energize particles to MeV energies in the cavity [*Chen and Fritz*, 1998; *Chen*, 2008]. *Chen* [2008] suggests that resonant acceleration via left-hand (with respect to the magnetic field) polarized ion cyclotron waves can energize ions from keV to MeV energies in seconds.

[5] A large body of work has been done on the wave mode identification in the high-altitude cusps both up to electron cyclotron frequency [*Pickett et al.*, 2001, 2002; *Blecki et al.*, 2005] and at the vicinity of ion cyclotron (IC) frequency [*Le et al.*, 2001; *Nykyri et al.*, 2003, 2004; *Sundkvist et al.*, 2005; *Grison et al.*, 2005; *Nykyri et al.*, 2006]. The fluctuations are typically broadband in nature but show intervals with wave trains at the vicinity of IC frequency and with clear polarization signatures during some wave periods. However, all of the studies listed above at the IC range are during "gradual" cusp crossings where the magnetic field, unlike for the diamagnetic cavity events, does not drop rapidly but changes gradually from ~120 nT to ~40 nT. Also for all of these cases the highest wave power at the vicinity of the local IC frequency occurs during the times when background magnetic field is still quite strong and plasma beta is very low, so the wave generation mechanisms and properties for these two different classes of cusp crossings (gradual cusp or diamagnetic cavity) may be quite different due to strongly different plasma betas. *Le et al.* [2001] suggested strong field-aligned flows and counter-streaming ions as a wave generation mechanism at the vicinity of local IC frequency and *Nykyri et al.* [2003] also

[1]Department of Physical Sciences, Embry-Riddle Aeronautical University, Daytona Beach, Florida, USA.
[2]Geophysical Institute, University of Alaska Fairbanks, Fairbanks, Alaska, USA.
[3]EISCAT Scientific Association, Kiruna, Sweden.

0148-0227/11/2010JA015888

suggested that gradients in the parallel flow could give free energy for these fluctuations to grow.

[6] During a "gradual" cusp wave event *Nykyri et al.* [2004] reported quite constant plasma temperatures of 1.5–3 MK and *Grison et al.* [2005] showed that perpendicular temperature can increase from ~3 MK to 6.5 MK during an interval with enhanced wave activity at 1–10 Hz frequencies. However, during the present diamagnetic cavity event the temperatures can exceed 15 MK and are typically around 10 MK in the cavity, although the corresponding solar wind temperature is typical and only 0.1–0.2 MK. In addition to heated bulk plasma, the present event shows enhanced fluxes of high-energy (up to several hundreds of keV) electrons, protons and helium ions [*Nykyri et al.*, 2011]. The presence of this high-energy (above 40 keV) tail in particle distributions is characteristic for the cusp diamagnetic cavity [*Chen and Fritz*, 2005].

[7] The obvious question is: what is the heating mechanism in the diamagnetic cavity? Are the particles locally heated or does the heating occur in the bow shock or magnetosphere but are just observed in the DMC? *Chen* [2008] suggested that if the wave electric fields are of the order of 50–100 mV/m ion acceleration up to MeV energies is possible.

[8] In the present paper it is demonstrated that not all fluctuations in the diamagnetic cavity are waves nor can be called "turbulence" in the traditional sense of the word. Media that is turbulent has many different scales that are in nonlinear interaction. Turbulence is characterized by various power laws for different types of turbulence: e.g., −5/3 for incompressible fluid turbulence [*Kolmogoroff*, 1941] which surprisingly is the power law observed also for the solar wind magnetic field power spectra. The isotropic magnetohydrodynamic (MHD) turbulence should show power laws of −3/2 [*Kraichnan*, 1995]. The reason for this discrepancy is not understood but one possible reason could be that solar wind is not adequately homogeneous but turbulence is localized in the magnetic flux tubes. Indeed, *Borovsky* [2008] showed that solar wind consists of magnetic flux tubes that are on average aligned with the Parker spiral, with a large spread in orientations. These flux tube boundaries could generate higher power at lower frequencies resulting possibly in steeper slope than −3/2.

[9] *Nykyri et al.* [2006] showed that slopes for the magnetic field power spectra in the high-altitude "gradual" cusps are highly variable, ranging from −2 to −1 below proton cyclotron frequency and from −5 to −3 above proton cyclotron frequency. Cusps also are not homogeneous but can have steep gradients in the density, flow and magnetic field [*Nykyri et al.*, 2004], which together with observed wave activity can result in vastly varying slopes.

[10] *Nykyri et al.* [2011] showed that dynamics and location of the diamagnetic cavity region is strongly influenced by solar wind. Using the word turbulence in reference to magnetic field fluctuations within DMC is therefore misleading: any period that is of the order of typical travel time through the cavity cannot be called turbulence in the traditional sense of the word. Simulation results by *Adamson et al.* [2011] indicate that while the cavity region can be extended in x, y direction several R_E it can be approximately a thousand kilometers wide in some regions. The fast magnetosonic speed in the cavity can exceed 1000 km/s (see Figure 1), setting the lowest frequency limit of turbulence to ~1 Hz.

[11] In section 4 we demonstrate that the majority of the low-frequency fluctuations in the DMC are in fact motion of the structure over the spacecraft: back and forth motion of the cavity boundaries and motion of the transient reconnection signatures, flux transfer events (FTEs). We also found signatures of clearly polarized wave structures at the vicinity of local proton cyclotron frequency and below, but unlike during the "gradual" cusp events reported by *Nykyri et al.* [2004], these waves are isolated showing only one oscillation and thus did not form regularly organized wave trains.

2. Instrumentation and Data Analysis Tools

[12] We use data from three instruments on Cluster spacecraft. Cluster is a four spacecraft multi-instrument constellation traveling in tetrahedron formation with variable spacecraft separation. For this event, the spacecraft separation is about ~5000 km enabling for the first time simultaneous observations of the diamagnetic cavity and surrounding boundaries.

[13] From each spacecraft, we use magnetic field measurements from the Fluxgate Magnetometer (FGM) [*Balogh et al.*, 2001], with a sampling rate of 4 vectors/s and 22.4 Hz for high-resolution data used in wave mode identification and power spectral calculations; ion spectra and moments from the Cluster Ion Spectrometer (CIS) [*Rème et al.*, 2001] from spacecraft 1 (sc1), 3 (sc3) and 4 (sc4). We use 4 s time resolution data for temperature, velocity and density from the Hot Ion Analyzer (HIA) which is part of CIS on sc1 and sc3. The HIA data has some data gaps that are linearly interpolated. The proton velocity, temperature and densities for sc4 are obtained from the ion Composition and Distribution Function analyzer (CODIF) which is also part of CIS for every 4 s and 8 s during some intervals.

[14] Our data analysis tools use the de Hoffman–Teller (HT) analysis and the Walén relation [*Sonnerup et al.*, 1995]. The HT frame is a frame where the convection electric field vanishes, thus indicating an approximately steady state plasma configuration. The HT velocity, $\mathbf{v_{HT}}$, is determined by minimizing $|(\mathbf{v} - \mathbf{v_{obs}}) \times \mathbf{B_{obs}}|^2$ in terms of the constant transformation velocity $\mathbf{v}$ for a given data set [*Sonnerup et al.*, 1995].

[15] The Walén relation is calculated in the HT frame as $\mathbf{v} - \mathbf{v_{HT}} = \pm\, C\, \mathbf{v_A}$ and implies that in the HT frame the plasma flow velocity is Alfvénic [*Sonnerup et al.*, 1995]. The Alfvén velocity, $\mathbf{v}_A = \mathbf{B}/\sqrt{(\mu_0 n_p m_p)}$, is corrected by factor $C = \sqrt{(1-\alpha)}$, where $\alpha = (T_{\parallel} - T_{\perp}) n_p k_B \mu_0 / B^2$ is the pressure anisotropy correction [e.g., *Sonnerup et al.*, 1981]. Walén relation is satisfied for Alfvén waves, rotational discontinuities, but also approximately for intermediate and switch-off slow shocks. These are often associated with magnetic reconnection.

[16] The boundary normal directions are calculated using the minimum variance of the magnetic field (MVAB), maximum variance of the electric field (MVAE) [*Sonnerup and Scheible*, 1998] and Minimum Faraday Residue (MFR) method [*Khrabrov and Sonnerup*, 1998]. The results for each boundary crossing using these three techniques are given by *Nykyri et al.* [2011]. For our event, the dominant

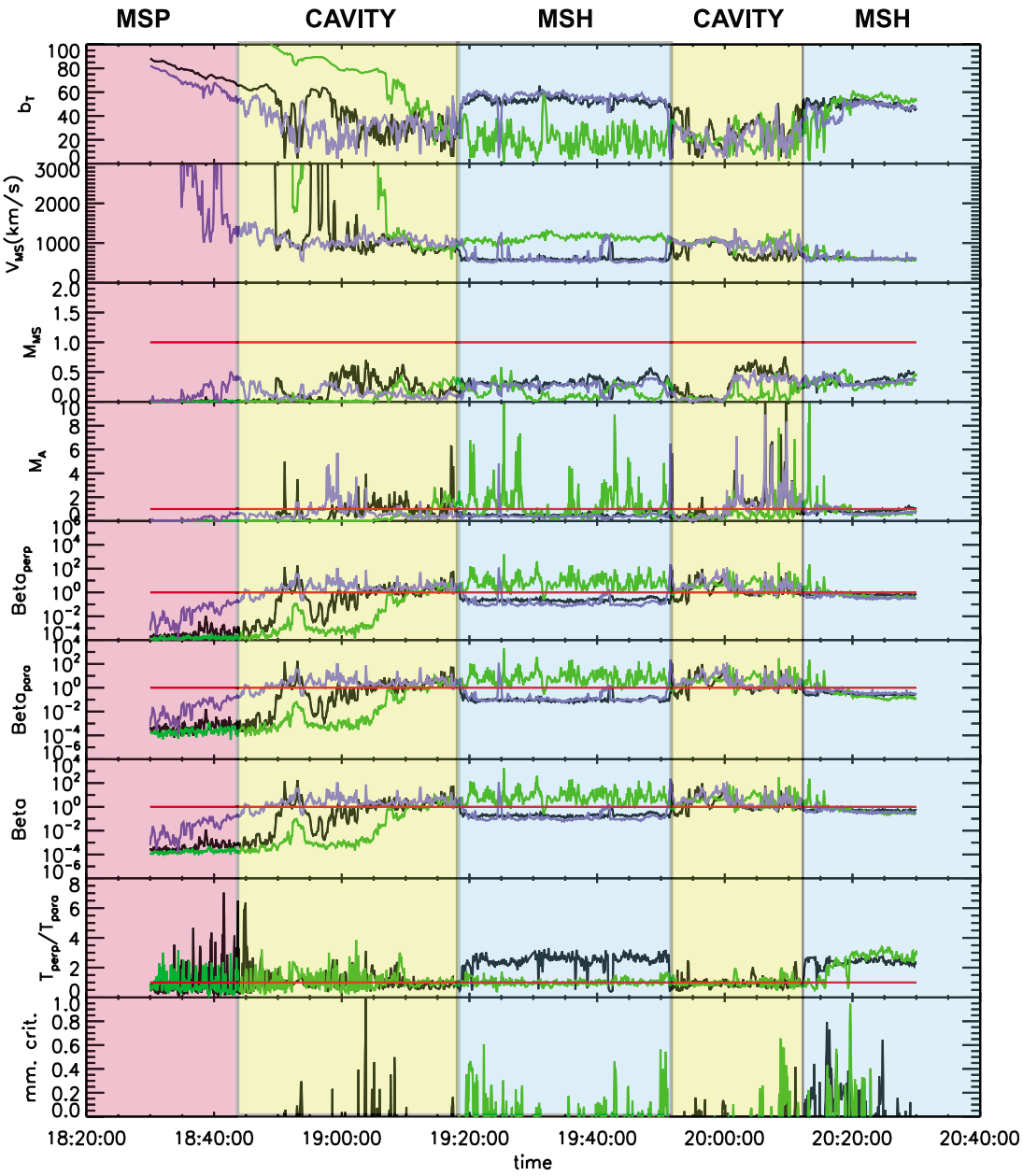

Figure 1. Cluster measurements for sc1 (black), sc3 (green), and sc4 (blue) of plasma parameters between 1830 and 2030 UT. The highlighted columns mark sc4 encounters with the cavity and surrounding regions. From top to bottom are magnetic field magnitude, magnetosonic speed, magnetosonic Mach number, Alfvén Mach number, perpendicular beta ($\beta_\perp$), parallel beta ($\beta_\parallel$), beta (β), plasma temperature ratio ($T_\perp/T_\parallel$), and mirror mode criteria ($T_\perp/T_\parallel - 1/\beta_\perp - 1$). The red horizontal line marks the level of unity. For sc4 we have only $T_\perp = T_\parallel$ available in the data.

magnetic field and the dominant plasma velocity are tangential to the boundary layer such that the maximum variance for the convection electric field should be normal to the layer which is the reason why MVAE test typically has the best performance for this event. This is why we use MVAE normal components in this article.

3. Overview of the Cusp Encounter

[17] Figure 1 shows a brief overview of plasma parameters during diamagnetic cavity and magnetosheath crossings between 1820 and 2040 UT (see caption for details on layout).

[18] The diamagnetic cavity (DMC) is characterized with depressed magnetic field, enhanced magnetic field fluctuations and enhanced plasma beta. The plasma beta exceeds 100 during many of the intervals. The magnetosonic speed increases at the magnetospheric boundary. The Alfvén Mach number is less than one in the magnetosheath and can be even 10 during some intervals in the cavity, during the intervals of fast reconnection flows. Here the spacecraft separation is ~5000 km, so we cannot say how filamentary

the reconnection flows are but *Nykyri et al.* [2003, 2004] illustrate that parallel field aligned flows can indeed be localized into very small scales having gradients of 100–600 km at the magnetospheric boundary in the high-altitude cusp. *Nykyri et al.* [2003] suggested that the gradients of the field-aligned flows could generate some of the observed wave activity at the vicinity of the high-altitude cusp. However, the plasma beta for the events abased in the works by *Nykyri et al.* [2003, 2004] is below one because spacecraft did not cross into diamagnetic cavity. Thus waves and their origin for these two different classes of cusp crossings may be different due to strongly different betas.

[19] Figure 1 also shows that the perpendicular temperature is larger in the magnetosheath, and in the cavity both perpendicular and parallel temperature can dominate during some intervals. The temperature anisotropy can give free energy for low-frequency fluctuations to grow. The mirror mode criteria, $T_\perp/T_\parallel - 1/\beta_\perp - 1$ [*Hasegawa*, 1969; *Siscoe*, 1983], is indeed greater than zero and thus satisfied during some intervals in the cavity and during the part of the latter magnetosheath interval.

[20] A typical signature for mirror mode waves is an anticorrelation between plasma density and magnetic field strength [see, e.g., *Soucek et al.*, 2008, and references therein]. Figure 2 shows plasma number density, *B* field magnitude, plasma temperature, plasma pressure and total pressure between 1830 and 1930 UT (Figure 2a) and at 1930–2030 UT (Figure 2b). Blue (pink) vertical lines refer to sc4 (sc1) intervals when there is anticorrelation (indicated by a), correlation (indicated by c) and no clear anticorrelation or correlation (indicated by n) between magnetic field strength and plasma number density. Although, the large-scale structure of the diamagnetic cavity for the present event can also be distinguished from magnetosphere by depressed magnetic field and enhanced plasma density similar to observations of *Niehof et al.* [2008], we did not a find a clear anticorrelation between some of the fluctuations of magnetic field magnitude and plasma density in the cavity. The presence of a large-amplitude density variations (~0.1–10/cc) and better anticorrelation between magnetic field magnitude and plasma density at the magnetosphere-cavity boundary compared to second cavity interval between ~1950 and 2020 UT can be associated with back and forth motion of the msp-cavity boundary by the spacecraft due to variations in dynamic pressure of the solar wind. The density between cavity and magnetosphere differs by two orders of magnitude (~0.1–10/cc) and multiple encounters of this msp-cavity boundary can be most clearly seen at sc1 between 1850 and 1907 UT. As spacecraft move further away from this inner boundary they encounter intervals where the amplitude of density variations is reduced and density minimum is higher (above 2/cc)(see intervals between 1905 and 1919 UT) and the anticorrelation between density and magnetic field is not always clear. For example at ~1942 UT, ~1953:30 UT and ~2001 UT sc1 observes a dip both in density and *B* field magnitude (correlation instead of anticorrelation) and one can see that there is a local peak in plasma temperature, so the decreased magnetic pressure is somewhat balanced by plasma pressure due to enhanced temperature. However, as can be seen in the fifth panels in Figures 2a and 2b, the pressure balance is not perfect anywhere. This is probably because thermal protons only provide part of the plasma pressure. It was demonstrated by *Nykyri et al.* [2011] that in addition to thermal and high-energy (above 40 keV) protons there are also significant fluxes of energized oxygen and helium ions observed during this event that would contribute to plasma pressure.

[21] The fact that the anticorrelation between *B* field magnitude and plasma number density is not so clear during some of the intervals in the cavity may suggest that these fluctuations are not mirror mode waves or simple back and forth motion of the msp-cavity boundary by the spacecraft. It will be demonstrated in section 4.2 that one of these signatures that lack this clear anticorrelation is likely a flux transfer event. However, the existence of mirror mode waves in the high-latitude magnetosheath may be important for the dynamics of the diamagnetic cavities as they will strongly modify the local magnetic field structure and thus the reconnection topology which will result likely in the modification of the reconnection rate and site.

[22] See *Nykyri et al.* [2011] for a detailed analysis of the structure and dynamics of the diamagnetic cavity. Here we only focus on the analysis of the magnetic field fluctuations in the DMC.

4. On the Origin of Fluctuations in the Diamagnetic Cavity: Waves or Structure?

[23] The magnetic field data in Figure 1 shows that diamagnetic cavity is filled with magnetic field fluctuations. Understanding the nature of these fluctuations is important as in some cases particles can gain energy from time varying electric and magnetic fields for example via cyclotron resonance or due to electric fields in kinetic Alfvén waves. However, what might look like turbulence in time series can also be spatial structure moving by the spacecraft such as flux transfer events or back and forth motion of the cavity boundary over the spacecraft due to variation in dynamic pressure of the solar wind [*Nykyri et al.*, 2011].

4.1. Identifying the Back and Forth Motion From the Transient Reconnection Signatures

[24] Figure 3 illustrates the nature and origin of low-frequency fluctuations at the magnetosphere diamagnetic cavity (MSP-DMC) boundary at 1848:40–1856:00 UT (Figure 3a) and during the first cavity interval at 1857:30–1922:00 UT (Figure 3b) observed by sc1 (see caption for more details on layout). During both intervals the magnetic field magnitude shows large-scale variations of the order of dB/B ~1 in a time scale of 30–90 s.

[25] After testing the method with different interval lengths, we have used a 30 s window. Each window is shifted by 6 s from the beginning of the previous window to calculate the MVAE normals during each of these intervals showing magnetic field variations and present these boundary normals in GSM coordinates. The 30 s window is short enough to capture the orientation of the structure for each fluctuation in the magnetic field and long enough to have adequate amount of data points for analysis. If a longer window was chosen one would average over several structures and the time variation of the normals would be less clear. Figure 3 shows the three components of the boundary normal, the total magnetic field, the maximum to intermediate Eigenvalue ratio, and the normals with Eigenvalue ratios larger than 4 for the time sliding window. Note that

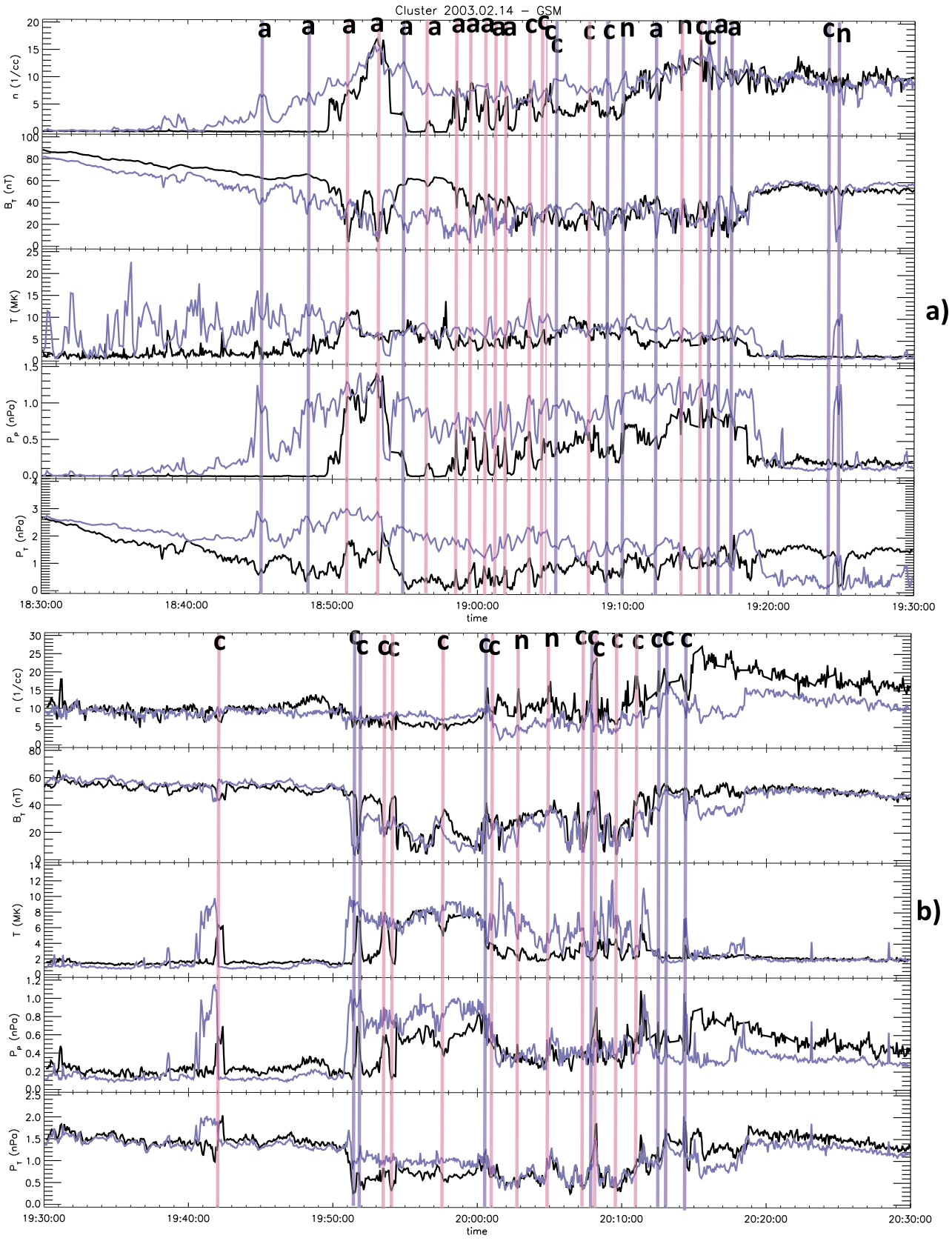

Figure 2. Plasma number density (n), B field magnitude (B_T), plasma temperature (T), plasma pressure (P_P), and total pressure (P_T) (a) between 1830 and 1930 UT and (b) at 1930–2030 UT. Blue (pink) vertical lines refer to sc4 (sc1) intervals when there is anticorrelation (indicated by a), correlation (indicated by c), and no clear anticorrelation or correlation (indicated by n) between B_T and n.

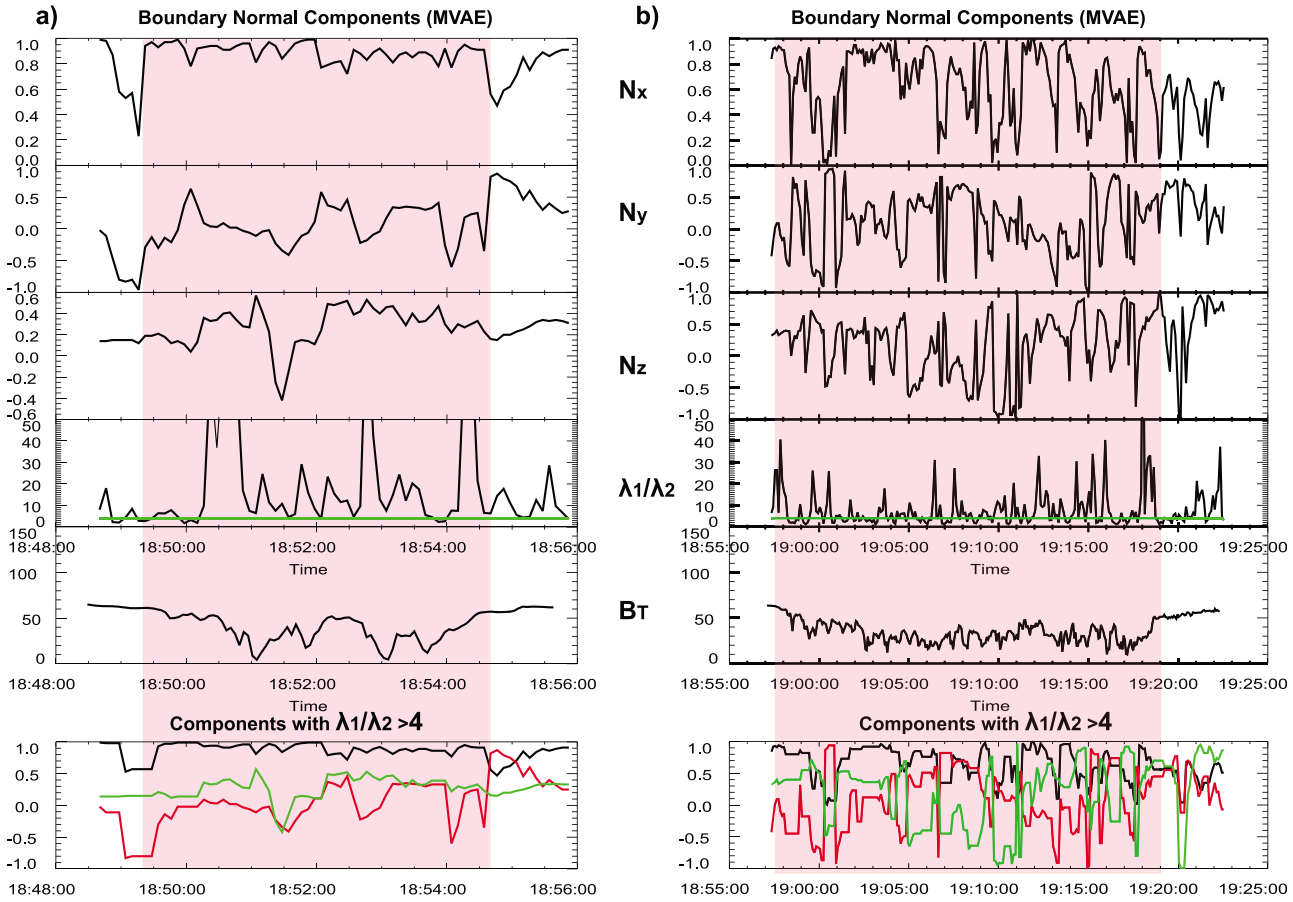

Figure 3. Sc1 observations of boundary normal components of the MVAE test, maximum and intermediate eigenvalue ratio (λ_1/λ_2), magnetic field magnitude, and boundary normal components for $\lambda_1/\lambda_2 > 4$ (a) for magnetosphere-cavity boundary at 1848:40–1856:00 UT and (b) for first cavity interval at 1857:30–1922:00 UT. Note that during the crossings of the inner boundary the x component of the normal, N_x, does not vary much, whereas in the cavity there is significantly more variability.

normals are physically significant only if the Eigenvalue ratio is sufficiently large.

[26] For the inner boundary (MSP-DMC) the x component of the boundary normal, N_x, is dominant and shows very little variation whereas in the cavity N_x varies more but shows also a region closer to the inner boundary at 1902–1906 where it is quite steady.

[27] The fact that the normal orientation for each of these 30 s intervals at the inner boundary remains nearly the same strongly suggests that sc1 encountered the same boundary several times. This is also consistent with the large-amplitude density variations(0.1–10/cc) that show anticorrelation with magnetic field magnitude (see Figure 2a and discussion in section 3). This back and forth motion of MSP-DMC boundary is likely due to dynamic pressure variations in the solar wind. The large-scale fluctuations in the cavity can be due to back and forth motion of the cavity magnetosheath (DMC-MSH) boundary and transient reconnection signatures. *Nykyri et al.* [2011, Table 1] indeed illustrate that between 1859 and 1920 UT sc1 encounters 15 reconnection intervals and between 1849 and 1856 none. The example reconnection intervals shown by *Nykyri et al.* [2011] illustrate that these intervals show fluctuations in magnetic field components. *Nykyri et al.* [2011] also showed that the DMC-MSH boundary is a rotational discontinuity and many of the FTEs at the DMC-MSH boundary have very strong N_z and small N_x components. One can see in Figure 3 that typically as the x component of the normal gets small, the z component gets large, consistent with transition from DMC into MSH.

[28] Also a statistical study of the properties of the exterior cusp has shown that the magnetic field fluctuations are associated with the magnetic shear angle, which may indicate that the large-amplitude fluctuations in the high-latitude exterior cusp region are mostly produced by the high-altitude reconnection process [*Zhang et al.*, 2005]. Our observations of reconnection signatures in the present paper and in the work by *Nykyri et al.* [2011] are in agreement with this result.

[29] In the following we will study these fluctuations in more detail and show another example of a flux transfer event at the magnetosheath-cavity boundary which creates a strong variation in magnetic field magnitude but also show examples of real plasma waves in the cavity.

4.2. Search and Analysis of Plasma Waves in the Cavity

[30] Figure 4 shows a spectrogram of magnetic field fluctuations between 1830 and 2030 UT. The white line shows

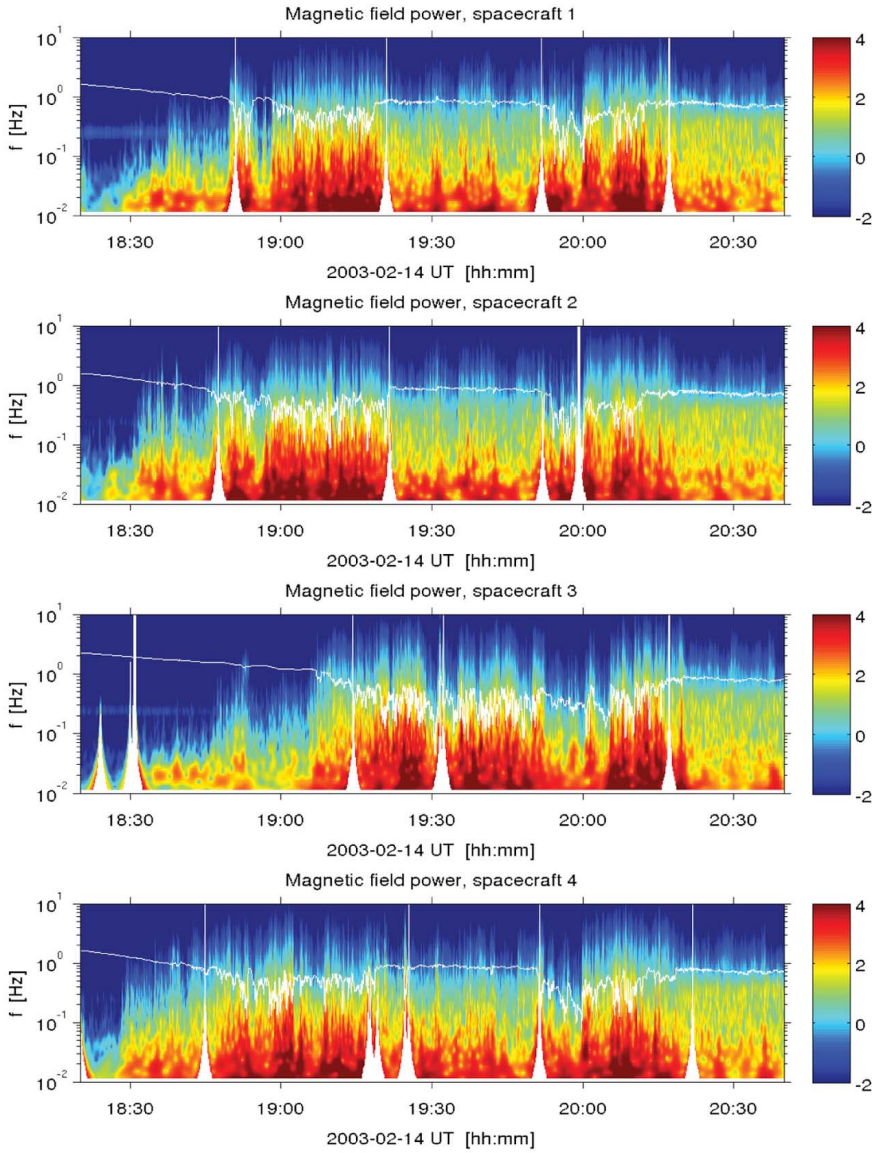

Figure 4. Power (in units of 10-logarithm of nT^2/Hz) of magnetic field fluctuations measured by four Cluster spacecraft as a function of time and frequency between 1830 and 2030 UT. Local proton cyclotron frequency is marked with white line.

the local proton cyclotron frequency which also nicely marks the diamagnetic cavity regions where the B field and thus the proton ω_{cp} cyclotron frequency are reduced. It is clear that most power (dark brown color) is between 0.01 and 0.1 Hz, which is typically below the local proton cyclotron frequency. However, the plasma flow speed in the cavity can be ≈600 km/s [*Nykyri et al.*, 2011]. In the regions of these enhanced flows the frequency of ion cyclotron waves is Doppler shifted according to

$$f_{SC} = \frac{1}{2\pi}(Vk\cos(\theta_{kV}) + \omega_{ci}) \quad (1)$$

where k is the wave number and θ_{kV} is the angle between the k vector and the plasma velocity. It is also possible that some Doppler shifted spatial structures are present.

[31] In order to test whether the low-frequency waves could be Doppler-shifted proton cyclotron waves we will calculate the maximum Doppler shift using equation (1). We can see that in order to get a reduced frequency in spacecraft frame (f_{SC}), the plasma flow velocity needs to be antiparallel to k vector of the wave. Using $V_{||} = -600$ km/s and k between 0.0013 and 0.0628 (corresponding to wavelengths of 5000–100 km), f_{SC} can be between 0.18 Hz (left hand polarized) and 5.7 (right hand polarized) for $f_{ci} = 0.3$ Hz, so it is possible that these could be Doppler shifted proton cyclotron modes. However, there are also many intervals when plasma flow velocity is only ≈50 km/s yielding left-hand polarized fluctuations with $f_{SC} = 0.29$–0.05 Hz (for wavelengths of 5000–200 km, respectively) excluding the proton cyclotron modes as the source for 1–1.5 min oscil-

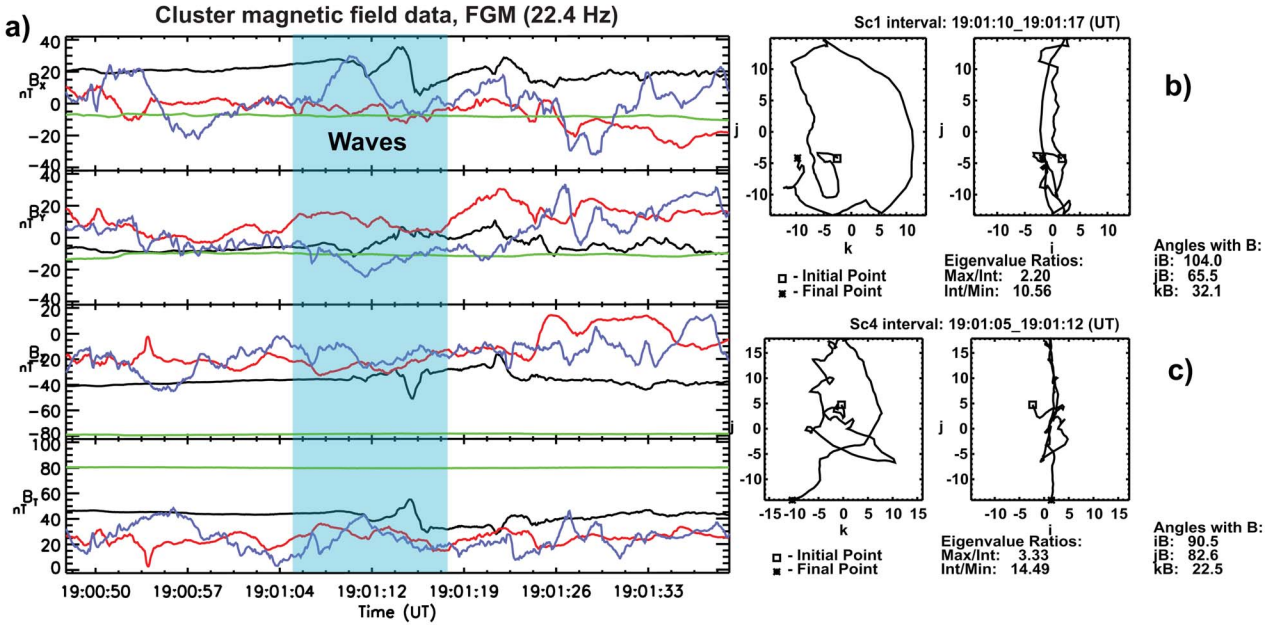

Figure 5. (a) High-resolution (22.4 Hz) magnetic field measurements between 1900:48 and 1901:40 UT. The light blue column highlights two large-amplitude waves for sc1 and sc4. The hodograms of these waves for (b) sc1 and (c) sc4. The minimum variance direction is into the paper, and magnetic field is coming out of the paper. The square (asterisk) is the beginning (end) of the wave interval, so both of these waves are left-handed in the spacecraft frame, but when taking into account the observed flows these can be right-handed in the plasma frame.

lations during these intervals for wavelengths equal or greater than 200 km. As illustrated in Figure 3 and by *Nykyri et al.* [2011], these large-scale variations can be caused by back and forth motion of the cavity boundary and motion of the FTEs over the spacecraft.

[32] In order to identify ion cyclotron modes in the high-resolution FGM (22.4 Hz) data, the search for the wave intervals is automated so that a 1, 5, 10, 30, 50, 70, 90 s window slides over the data sets of all four spacecraft with a 10% shift of the interval length. Minimum variance analysis [*Sonnerup and Scheible*, 1998] is used for each search interval to present the wave magnetic field in directions of maximum (j), intermediate (k) and minimum (i) variance and all the wave intervals with intermediate/minimum eigenvalue ratios greater than 10 are selected [*Eastwood et al.*, 2002]. The absolute value of wave ellipticity, e, is defined as a square root of the intermediate and maximum eigenvalue ratio. For circularly polarized waves e should be 1 and for linearly polarized waves 0. We have required that $|e|$ is larger than 0.5 in order to pick up elliptically and circularly polarized waves. The sign of polarization is determined from hodogram and the angle between minimum variance and magnetic field direction.

[33] With this search criteria we found several hundred 1 s wave intervals for all spacecraft moving with various angles with respect to background magnetic field ranging from nearly parallel to perpendicular. The majority of these show clear left- and right-handed polarizations, but there are also several intervals where clear polarization is absent. For larger wave periods there are significantly more intervals that do not show clear polarizations due to higher-frequency noise, for example the 90 s search window yields only one wave interval with clear polarization: a right-handed wave for sc1 observed between 1831:20 and 1832:50 UT. The wave amplitudes for most intervals are around 1–2 nT but we have also found highly nonlinear waves with amplitudes of ≈10–30 nT. Figure 5a shows two examples of large-amplitude waves observed by sc1 (black curve) and sc4 (blue curve) highlighted with light blue column. In the hodogram plots the minimum variance direction is into the paper, so both of these waves are left-handed in the spacecraft frame as the angle between background magnetic field and minimum variance direction is greater than 90°. Between 1901:00 and 1901:30 UT sc1 and sc4 measure average flow velocities of ≈[231., −169., −410.]km/s and ≈ [75., −190., −148] km/s, respectively, so these frequencies will be Doppler shifted. Sc1 observes this wave during enhanced reconnection flows [*Nykyri et al.*, 2011]. The angle between wave propagation direction (i) and velocity vectors, θ_{kV}, are 121.° and 106.° for sc1 and sc4, respectively. Plugging these values into equation (1), using 7 and 5 s periods for sc1 and sc4 and assuming the local observed ω_{ci} (3.9 rad/s for sc1 and 2.05 rad/s for sc4), these waves could be nonlinear kinetic right-handed magnetosonic modes in plasma frame if the wavelengths are below 350 km and 130 km for sc1 and sc4, respectively. If these waves originate from region of lower magnetic field, the wavelengths can be even larger to be considered as kinetic magnetosonic modes. The cross-correlation coefficients of the magnetic field observed by sc1 and sc4 between 1901:05 and 1901:17 UT are below 0.43 for all the components and the time shifts for yielding the best correlations vary between different components, so it can be concluded that the observed wavelengths are less than spacecraft separation

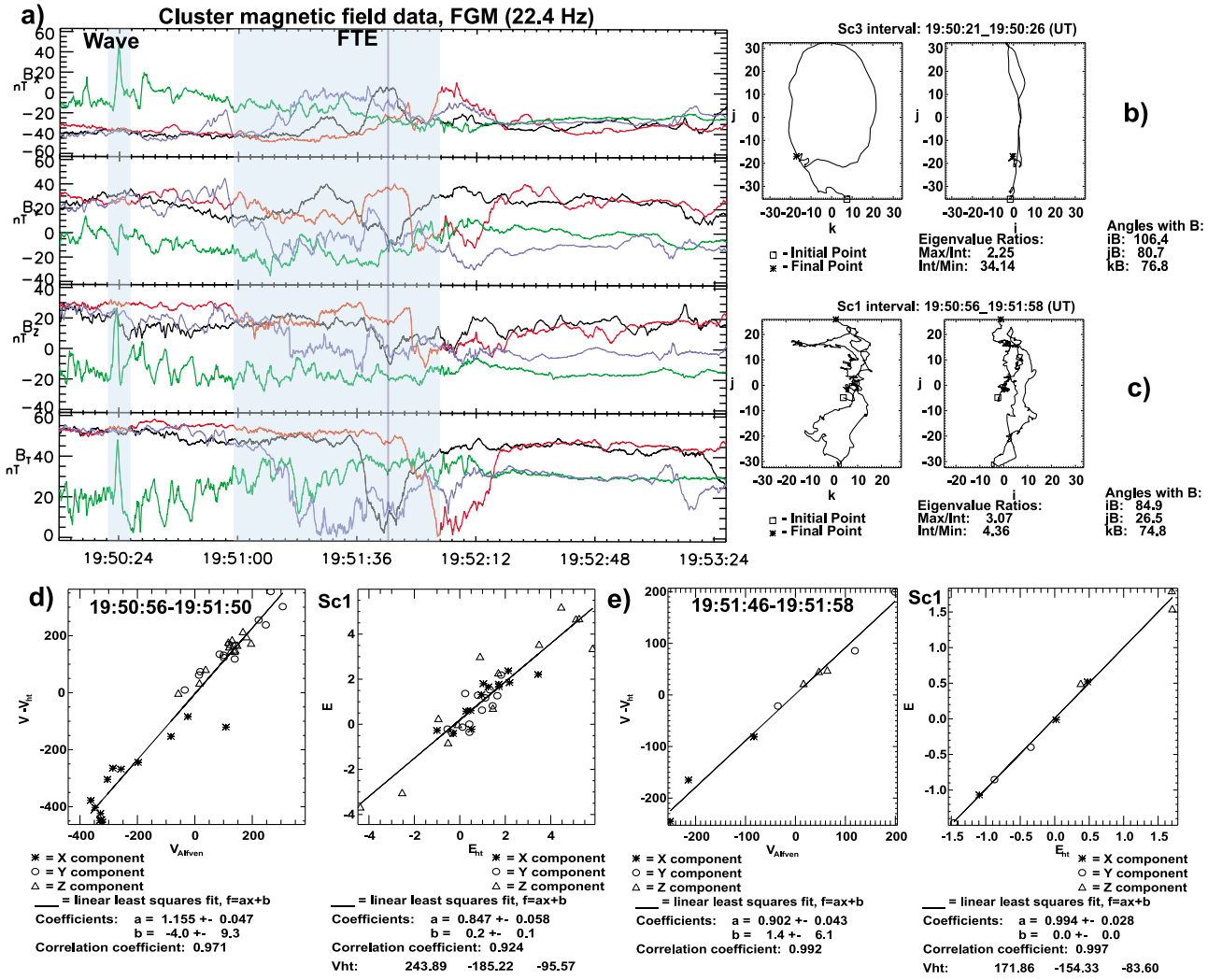

Figure 6. (a) High-resolution (22.4 Hz) magnetic field measurements between 1950:08 and 1953:28 UT. The first light blue column highlights a large-amplitude wave observed by sc3 at 1950:21–1950:26 UT, and the second light blue column highlights two overlapping intervals at 1950:56–1951:58 UT when sc1 observes good Walén relations and HT frames (also reported by *Nykyri et al.* [2011, Table 2]). The hodograms for these intervals for (b) sc3 and (c) sc4. The scatterplots for Walén relations and HT frames observed by sc1 (d) between 1950:56 and 1951:50 and (e) between 1951:46 and 1951:58 UT. The blue vertical line shows approximately the end and beginning of the first and second variance intervals (Figures 6d and 6e), respectively.

projected along the wave propagation direction, which are 250 km and 3170 km for sc1 and sc4, respectively. With the absence of high-resolution plasma data we also cannot rule out the possibility that these could be small-scale magnetic flux ropes generated by reconnection process. However, many of the intervals described for this event by *Nykyri et al.* [2011] that have good Walén relations and HT frames have S-shaped hodograms [see, e.g., *Nykyri et al.*, 2011, Figure 7] or are lacking a clear polarization signature, making the nonlinear kinetic magnetosonic modes a viable explanation for these large-amplitude magnetic field oscillations.

[34] More examples of the analysis of the "turbulence" in the cavity are shown in Figure 6 (see caption for more detail on format). High-resolution magnetic field data and MVAB hodograms indicate that sc3 observes a highly nonlinear structure which is left-handed polarized in spacecraft frame, but plasma flows of ≈240 km/s measured at 1950:21–1950:26 UT can change the polarization to right-handed in plasma frame according to equation (1). This could be a nonlinear magnetosonic mode similar to ones observed in Figure 5 or a filamentary flux rope. Note that this signature is not even present in spin-averaged data. We have run 1-D MHD simulations (not shown) that indicate that for the observed nonlinear perturbations large-amplitude waves can be generated that steepen rapidly into shock structures.

[35] Between 1951 and 1952:30 UT sc1, sc2 and sc4 all observe a similar structure (slightly time shifted) characterized by a drop in magnetic field strength and increased plasma beta (see Figure 1) and subsequent recovery almost back to the initial level (expect for sc4 for which the recovery is less complete). This signature cannot be explained by a simple back and forth motion of the 1-D cavity boundary

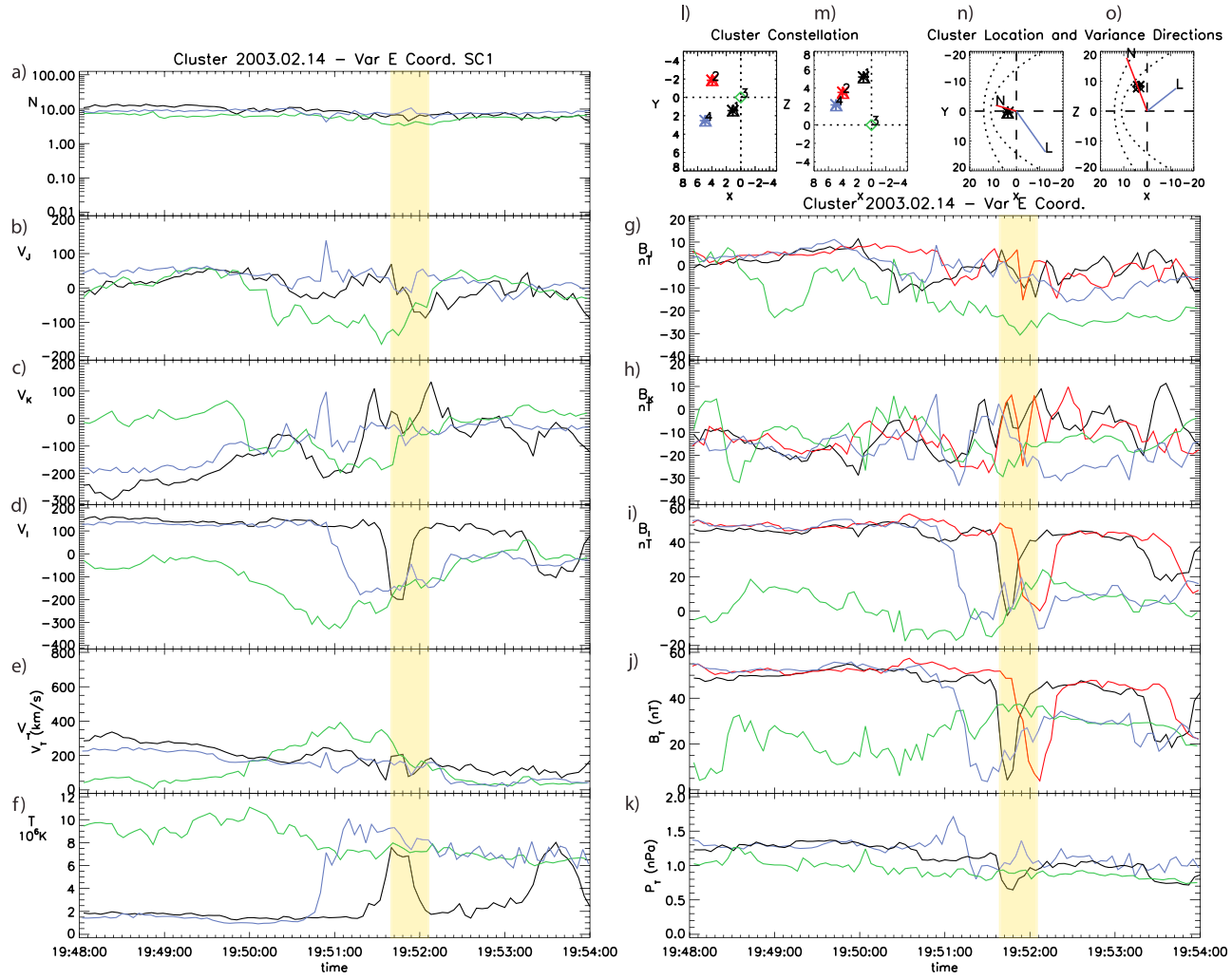

Figure 7. Cluster plasma and magnetic field data on 14 February 2003 between 1948 and 1954 UT rotated into MVAE coordinates (*j*, *k*, and *i* corresponding to maximum (normal), intermediate, and minimum variance direction) calculated by sc1between 1942 and 2000 UT. (a–f) Plasma density, three components of plasma velocity, total velocity, and plasma temperature. (g–k) Three components of the magnetic field, total magnetic field and total pressure. Also shown are Cluster separation (units are in thousands of kilometers) from sc3 projected at (l) *xy* plane and (m) *xz* plane and Cluster location (units are in Earth radius) at (n) *xy* plane and (o) *xz* plane. The approximate magnetopause and bow shock locations are drawn as parabolas together with projections of MVAE boundary normal (red line) and tangent (blue line).

because this is not a nested structure. Existence of the good Walén relations and HT frames for both sides of this structure measured by sc1 suggests that this is possibly a reconnection event moving by sc1 and later encountered by sc2. Even for the combined time interval 1950:56–1951:58 UT (scatterplot not shown) the slopes of Walén relation and HT frame are 1.15 and 0.86, and correlation coefficients for Walén relations and HT frames are 0.97 and 0.93, respectively. The cross-correlation coefficients (ccc) calculated between different spacecraft pairs between 1950:56 and 1952:30 UT are highest for pair sc1-sc2 which is not a surprise when looking at the similar signatures they observe. The ccc's for this pair vary between 0.71 and 0.85 between different magnetic field components. The time lag corresponding to the best ccc is 19.6 s. Projecting the sc1 and sc2 separations along the unit vector along the de Hoffman–Teller frame velocity of [241, −185, −95] km/s measured during the combined interval between 1950:56 and 1951:58 UT and by dividing this separation with this HT speed gives a time of 14.5s. Applying the same analysis for de Hoffman–Teller frame velocities plotted in Figures 6d and 6e yields time lags of 14.4 and 19.0 s, respectively.

[36] We have also checked whether the structure in Figure 6c shows a bipolar signature of the normal component of the magnetic field by rotating the data in boundary normal coordinates calculated with MVAE technique for the data interval 1942–2000 UT measured by sc1. The components of this normal in GSM coordinates are [0.44, −0.1, 0.89] and λ_1/λ_2 is 13. The Cluster plasma and magnetic field data is rotated into this coordinate system and shown in Figure 7 (see caption for details on format). The normal component of the magnetic field between 1951:42 and

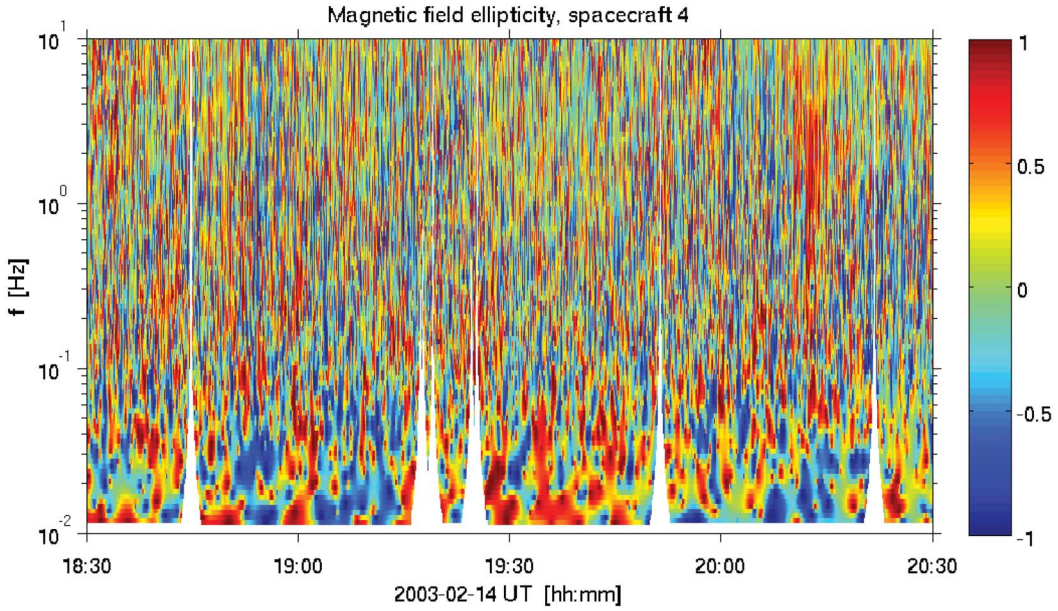

Figure 8. Ellipticity of magnetic field fluctuations measured by sc4. Red indicates right-handed waves, and blue shows left-handed waves. Green shows linearly polarized waves.

1952:05 UT changes from positive 5 nT to −15 nT (see highlighted yellow column in Figure 7g). In addition there is a local pressure imbalance associated with these signatures. One can see that the plasma temperature is enhanced when the peak in total pressure is observed (see blue trace for sc4 and black trace for sc1 between 1951 and 1952 UT) which is followed by a dip in total pressure as the magnetic field magnitude gets reduced.

[37] We interpret that this is a reconnection event consistent with a large-amplitude magnetic perturbation of Alfvénic nature and the presence of the good de Hoffman–Teller frame [*Sonnerup et al.*, 1995] with the possibility of it being an FTE that originates from reconnection site at duskside cusp and is moving sunward, earthward and dawnward and observed first at sc1 reaching sc2 about 14.4–19.0 s later. This can be easily visualized by looking at the cluster constellation at *y*-*x* and *z*-*x* planes in Figure 1 of *Nykyri et al.* [2011] and in Figures 7l–7o which shows that sc1 and sc2 are located almost along the direction of the propagation of the structure (along the HT frame velocity vector). The hodogram observed during this magnetic field perturbation at the longer time interval 1950:56–1951:58 UT looks like a distorted number eight. Now it is easy to see that by choosing this interval shorter at both ends one can find a S-shaped hodogram. The additional noise that is present in the hodogram in Figure 6c compared to those given by *Nykyri et al.* [2011] is due to higher resolution (22.4 Hz) used in former. However, choosing a larger time interval around 1950:21–1950:26 UT does not yield an eight-shaped or S-shaped hodogram for sc3. We think that either the physical mechanism generating the signature measured at sc3 is fundamentally different (could be a nonlinear magnetosonic mode) or sc3 is observing a flux rope which is showing a different signature because the ambient magnetic field conditions are different at sc3 location compared to those at sc1 and sc2.

[38] The background magnetic field used for determination of the wave polarization for the shown hodograms has been averaged over the duration of the wave interval. For example the direction of *k* vector for the 5 s interval determined in Figure 6b is [−0.07, 0.92,0.37] in GSM coordinates and angle between the *k* and *B* field during this 5 s period is 106.4°, so the wave propagates with 73.6° angle with respect to magnetic field. If the *B* field is averaged over 500% around the wave interval (25 s period) instead, the angle between the *k* and *B* field becomes 110.0°. For the wave interval reported in Figure 5a, the angle between *k* and *B* changes from 104.0° to 104.7° when the time interval for average *B* calculation is increased to 35 s, so for both of these cases the polarization of the wave does not change when longer time interval is considered for the average of the *B* field. For the intervals listed in Figures 5c and 6c, the background magnetic field lies roughly in the plane of oscillation, so that the structures propagate at very oblique angles (89.5° and 84.9°, respectively) from the local magnetic field. In these cases it is questionable to determine the wave polarization although the angle between B and k is not exactly 90°. These intervals were not even picked by the automated search for wave intervals but were analyzed due to their vicinity and similarity with respect to wave intervals listed in Figures 5b and 6b.

[39] In order to summarize the properties of wave intervals we present in Figure 8 the polarization calculations of magnetic field fluctuations measured by sc4 between 1830 and 2030 UT. The magnetic field data is transformed into a magnetic field aligned coordinate system and polarization of the wave magnetic field is calculated in that coordinate system using the method illustrated by *Carozzi et al.* [2001]. In order to determine polarization we have calculated a time series of the background magnetic field by removing the fastest fluctuations using a Empirical Mode Decomposition method. These calculations illustrate the general patchiness of wave polarization which was also

confirmed with our automated search method for different length wave intervals, so the wave polarization can change from one wave cycle to next. At around 2015 UT there is an interval with more right-handed polarizations in spacecraft frame but comparing this with the wave power plot presented in Figure 4 indicates that the wave power is very small during this interval above 1 Hz.

[40] The magnetic field power spectra from STAFF instrument (not shown) indicates that there is no significant wave power (power is typically less than 10^{-6} nT^2/Hz) at the vicinity of electron cyclotron frequencies from ~280 Hz to 1.7 kHz (calculated using magnetic field strengths of 10 nT and 60 nT). The magnetic and electric field wave power between 10 and 100 Hz are ~10^{-4} nT^2/Hz and ~10^{-2} mV^2/m^2 Hz, respectively, suggesting that the fluctuations at this range are mostly electrostatic ($E/B > v_A$). These fluctuations may be lower hybrid waves also observed in high-altitude cusp by *Blecki et al.* [2005]. Although lower hybrid waves are capable of accelerating ions [*Chang and Coppi*, 1981] and electrons [*Bingham et al.*, 1984] in ionospheric and auroral altitudes, the role and efficiency of these waves for particle acceleration and heating at high-altitude cusps remains to be shown.

5. Discussion and Conclusions

[41] In this paper it is demonstrated that not all magnetic field fluctuations in the diamagnetic cavity are waves or can be called turbulence. The magnetosonic speed in DMC is typically 1000 km/s setting the lowest frequency limit of turbulence to 0.2–1 Hz assuming that the length scales in the cavity can be as small as 1000–5000 km.

[42] The 30–60 s fluctuations at the magnetosphere-cavity (MSP-DMC) boundary are shown to be back and forth motion of the MSP-DMC boundary whereas the 30–90 s fluctuations in the cavity are shown to be mostly combination of transient reconnection signatures and back and forth motion of the cavity structure.

[43] We also found signatures of isolated plasma wave modes, possibly ion cyclotron and magnetosonic modes with small amplitudes but also found several isolated large-amplitude waves that were left-handed in the spacecraft frame but right-handed in the plasma frame. These were propagating closely perpendicular with respect to background field. Comparison with 1-D MHD simulations indicate that observed perturbations can generate large-amplitude waves that steepen rapidly into shock structures. The role that these isolated waves have in particle heating in the DMC is not currently understood. We did not observe such a large electric fields as were reported by *Chen* [2008] and who suggested that resonant acceleration via ion cyclotron waves could yield MeV energies in the DMC. *Chen* [2008] did not actually show the amplitude of the clearly polarized wave electric field but the large electric field magnitude that was shown was for a different event.

[44] Clearly, more work is needed in order to fully understand the role these waves play in the particle heating and acceleration in the DMCs. However, it can be concluded that (1) many of the observed fluctuations in the DMC are structure rather than waves, (2) There is very little wave power at and above local proton cyclotron frequency, and (3) observed waves were isolated showing typically only one wave cycle.

[45] These conclusions may suggest that wave heating at the vicinity of IC frequency for these DMC events is not as significant as for the "gradual" cusp event reported by *Grison et al.* [2005]. Waves may play important role in scattering though. Scattering is an energy-conserving process and may help in recycling the particles through gradients in reconnection "quasi-potential" if particles remain trapped for long enough time. Also, the role of the lower hybrid range fluctuations need to be further investigated for the DMC events.

[46] **Acknowledgments.** K. Nykyri's work is supported by National Science Foundation grant 0703327. We thank Cluster CIS and FGM teams for providing the well-calibrated Cluster data used in this study. We acknowledge the use of Cluster Active Archive for checking the STAFF magnetic field spectrogram for high-frequency fluctuations.

[47] Masaki Fujimoto thanks Jonathan Niehof and the other reviewers for their assistance in evaluating this paper.

References

Adamson, E., et al. (2011), 3D mesoscale MHD simulations of a cusp-like magnetic configuration: Method and first results, *Ann. Geophys.*, in press.

Asikainen, T., and K. Mursula (2005), Energetic particle fluxes in the exterior cusp and the high-latitude dayside magnetosphere: Statistical results from the Cluster/RAPID instrument, *Ann. Geophys.*, *23*, 2217–2230.

Asikainen, T., and K. Mursula (2006), Reconnection and energetic particles at the edge of the exterior cusp, *Ann. Geophys.*, *24*, 1949–1956.

Balogh, A., et al. (2001), The Cluster magnetic field investigation: Overview of in-flight perfomance and initial results, *Ann. Geophys.*, *19*, 1207–1217.

Bingham, R., D. A. Bryant, and D. S. Hall (1984), A wave model for the aurora, *Geophys. Res. Lett.*, *11*, 327–330.

Blake, J. B. (1999), Comment on "Cusp: A new acceleration region of the magnetosphere" by J. Chen et al., *Czech. J. Phys.*, *49*, 675.

Blecki, J., et al. (2005), Low-frequency plasma waves in the outer polar cusp: A review of observations from Prognoz 8, Interball 1, Magion 4, and Cluster, *Surv. Geophys.*, *26*, 177–191.

Borovsky, J. E. (2008), Flux tube texture of the solar wind: Strands of the magnetic carpet at 1 AU?, *J. Geophys. Res.*, *113*, A08110, doi:10.1029/2007JA012684.

Carozzi, T. D., B. Thidé, T. B. Leyser, G. Komrakov, V. Frolov, S. Grach, and E. Sergeev (2001), Full polarimetry measurements of stimulated electromagnetic emissions: First results, *J. Geophys. Res.*, *106*, 21,395–21,408.

Chang, S., et al. (1998), Cusp energetic ions: A bow shock source, *J. Geophys. Res.*, *25*, 3729–3732.

Chang, S., et al. (2000), Energetic magnetosheath ions connected to the Earth's bow shock: Possible source of cusp energetic ions, *J. Geophys. Res.*, *105*, 5471–5488.

Chang, T., and B. Coppi (1981), Lower hybrid acceleration and ion evolution in the suprauroral region, *Geophys. Res. Lett.*, *8*, 1253–1256.

Chen, J. (2008), Evidence for particle acceleration in the magnetospheric cusp, *Ann. Geophys.*, *26*, 1993–1997.

Chen, J., and T. A. Fritz (1998), Correlation of cusp MeV helium with turbulent ULF power spectra and its implications, *Geophys. Res. Lett.*, *25*(22), 4113–4116, doi:10.1029/1998GL900122.

Chen, J., and T. A. Fritz (2001), Energetic oxygen ions of ionospheric origin observed in the cusp, *Geophys. Res. Lett.*, *28*, 1459–1462.

Chen, J., and T. A. Fritz (2005), High-altitude cusp: The extremely dynamic region in geospace, *Surv. Geophys.*, *26*, 71–93.

Delcourt, D. C., and J. Sauvaud (1998), Recirculation of plasma sheet particles into the high-latitude boundary layer, *J. Geophys. Res.*, *103*, 26,521–26,532.

Delcourt, D. C., and J. Sauvaud (1999), Populating of the cusp and boundary layers by energetic (hundreds of keV) equatorial particles, *Geophys. Res. Lett.*, *104*, 22,635–22,648.

Eastwood, J. P., A. Balogh, M. W. Dunlop, T. S. Horbury, and I. Dandouras (2002), Cluster observations of fast magnetosonic waves in the terrestrial foreshock, *Geophys. Res. Lett.*, *29*(22), 2046, doi:10.1029/2002GL015582.

Frank, L. A., and K. L. Ackerson (1971), Observations of charged particle precipitation into the auroral zone, *J. Geophys. Res.*, *76*, 3612–3643.
Fritz, T., J. Chen, R. Sheldon, H. Spence, J. Fennell, S. Livi, C. Russell, and J. Pickett (1999), Cusp energetic particle events measured by POLAR spacecraft, *Phys. Chem. Earth C*, *24*, 135–140.
Grison, B., F. Sahraoui, B. Lavraud, T. Chust, N. Cornilleau-Wehrlin, H. Reme, A. Balogh, and M. Andre (2005), Wave particle interactions in the high-altitude polar cusp: A cluster case study, *Ann. Geophys.*, *23*, 3699–3713.
Hasegawa, A. (1969), Drift mirror instability of the magnetosphere, *Phys. Fluids*, *12*, 2642–2650.
Heikkilä, W. J., and J. D. Winningham (1971), Penetration of magnetosheath plasma to low altitudes through the dayside magnetospheric cusps, *J. Geophys. Res.*, *76*, 883–891.
Khrabrov, A. V., and B. Sonnerup (1998), Orientation and motion of current layers: Minimization of the Faraday residue, *Geophys. Res. Lett.*, *25*, 2373–2376.
Kolmogoroff, A. N. (1941), The local structure of turbulence in incompressible viscous fluid for very large Reynolds number, *Dokl. Akad. Nauk SSSR*, *30*, 301–305.
Kraichnan, R. H. (1995), Inertial-range spectrum of hydromagnetic turbulence, *Phys. Fluids*, *8*, 1385–1387.
Kremser, G., J. Woch, K. Mursula, P. Tanskanen, B. Wilken, and R. Lundin (1995), Origin of energetic ions in the polar cusp inferred from ion composition measurements by the Viking satellite, *Ann. Geophys.*, *13*, 595–607.
Lavraud, B., A. Fedorov, E. Budnik, A. Grigoriev, P. Cargill, M. Dunlop, H. Rème, I. Dandouras, and A. Balogh (2004), Cluster survey of the high-altitude cusp properties: A three-year statistical study, *Ann. Geophys.*, *22*, 3009–3019.
Lavraud, B., A. Fedorov, E. Budnik, M. F. Thomsen, A. Grigoriev, P. J. Cargill, M. W. Dunlop, H. Rème, I. Dandouras, and A. Balogh (2005a), High-altitude cusp flow dependence on IMF orientation: A 3-year Cluster statistical study, *J. Geophys. Res.*, *110*, A02209, doi:10.1029/2004JA010804.
Lavraud, B., et al. (2005b), Cluster observes the high-altitude cusp region, *Surv. Geophys.*, *26*, 135–175.
Le, G., X. Blanco-Cano, C. T. Russell, X.-W. Zhou, F. Mozer, K. J. Trattner, S. A. Fuselier, and B. J. Anderson (2001), Electromagnetic ion cyclotron waves in the high-altitude cusp: Polar observations, *J. Geophys. Res.*, *106*, 19,067–19,079.
Niehof, J. T., T. A. Fritz, R. H. W. Friedel, and J. Chen (2008), Interdependence of magnetic field and plasma pressures in cusp diamagnetic cavities, *Geophys. Res. Lett.*, *35*, L11101, doi:10.1029/2008GL033589.
Nykyri, K., P. J. Cargill, E. A. Lucek, T. S. Horbury, A. Balogh, B. Lavraud, I. Dandouras, and H. Rème (2003), Ion cyclotron waves in the high altitude cusp: CLUSTER observations at varying spacecraft separations, *Geophys. Res. Lett.*, *30*(24), 2263, doi:10.1029/2003GL018594.
Nykyri, K., et al. (2004), Cluster observations of magnetic field fluctuations in the high-altitude cusp, *Ann. Geophys.*, *22*, 2413–2429.
Nykyri, K., B. Grison, P. J. Cargill, B. Lavraud, E. Lucek, I. Dandouras, A. Balogh, N. Cornilleau-Wehrlin, and H. Réme (2006), Origin of the turbulent spectra in the high-altitude cusp: Cluster spacecraft observations, *Ann. Geophys.*, *24*,1057–1075.
Nykyri, K., A. Otto, E. Adamson, E. Dougal, and J. Mumme (2011), Cluster observations of a cusp diamagnetic cavity: Structure, size, and dynamics, *J. Geophys. Res.*, *116*, A03228, doi:10.1029/2010JA015897.
Pickett, J. S., J. R. Franz, J. D. Scudder, J. D. Menietti, D. A. Gurnett, G. B. Hospodarsky, R. M. Braunger, P. M. Kintner, and W. S. Kŭrth (2001), Plasma waves observed in the cusp turbulent boundary layer: An analysis of high time resolution wave and particle measurements from the Polar spacecraft, *J. Geophys. Res.*, *106*, 19,081–19,100.
Pickett, J. S., J. D. Menietti, G. B. Hospodarsky, D. A. Gurnett, and K. Stasiewicz (2002), Analysis of the turbulence observed in the outer cusp turbulent boundary layer, *Adv. Space Res.*, *30*, 2809–2814.
Rème, H., et al. (2001), First multispacecraft ion measurements in and near the Earth's magnetosphere with the identical Cluster ion spectrometry (CIS) experiment, *Ann. Geophys.*, *19*, 1303–1354.
Siscoe, G. L. (1983), Solar system magnetohydrodynamics, in *Solar-Terrestrial Physics: Principles and Theoretical Foundations*, *Astrophys. and Space Sci. Libr.*, vol. 104, edited by R. L. Carovillano and J. M. Forbes, pp. 11–100, D. Reidel, Dordrecht, Netherlands.
Sonnerup, B. U. Ö., and M. Scheible (1998), Minimum and maximum variance analysis, in *Analysis Methods for Multi-spacecraft Data*, *ISSI Sci. Rep., SR-001*, edited by G. Paschmann and P. W. Daly, pp. 185–220, Int. Space Sci. Inst., Bern.
Sonnerup, B. U. Ö., G. Paschmann, I. Papamastorakis, N. Sckopke, G. Haerendel, S. J. Bame, J. R. Asbridge, J. T. Gosling, and C. T. Russell (1981), Evidence for magnetic reconnection at the Earth's magnetopause, *J. Geophys. Res.*, *86*, 10,049–10,067.
Sonnerup, B. U. Ö., G. Paschmann, and T.-D. Phan (1995), Fluid aspects of reconnection at the magnetopause: In situ observations, in *Physics of the Magnetopause*, *Geophys. Monogr. Ser.*, vol. 90, edited by P. Song, B. U. Ö. Sonnerup, and M. F. Thomsen, pp. 167–180, AGU, Washington, D. C.
Soucek, J., E. Lucek, and I. Dandouras (2008), Properties of magnetosheath mirror modes observed by Cluster and their response to changes in plasma parameters, *J. Geophys. Res.*, *113*, A04203, doi:10.1029/2007JA012649.
Sundkvist, D., et al. (2005), Multi-spacecraft determination of wave characteristics near the proton gyrofrequency in high-altitude cusp, *Ann. Geophys.*, *23*, 983–995.
Trattner, K. J., S. A. Fuselier, W. K. Peterson, and S. Chang (1999), Comment on "Correlation of cusp MeV helium with turbulent ULF power spectra and its implications," *Geophys. Res. Lett.*, *26*, 1361–1362.
Trattner, K. J., S. A. Fuselier, W. K. Peterson, S.-W. Chang, R. Friedel, and M. R. Aellig (2001), Origins of energetic ions in the cusp, *J. Geophys. Res.*, *106*, 5967–5976.
Walsh, B. M., T. A. Fritz, N. M. Lender, J. Chen, and K. E. Whitaker (2007), Energetic particles observed by ISEE-1 and ISEE-2 in a cusp diamagnetic cavity on 29 September 1978, *Ann. Geophys.*, *25*, 2633–2640.
Walsh, B. M., T. A. Fritz, M. M. Klida, and J. Chen (2010), Energetic electrons in the exterior cusp: Identifying the source, *Ann. Geophys.*, *28*, 983–992.
Whitaker, K. E., J. Chen, and T. A. Fritz (2006), CEP populations observed by ISEE 1, *Geophys. Res. Lett.*, *33*, L23105, doi:10.1029/2006GL027731.
Whitaker, K. E., T. A. Fritz, J. Chen, and M. Klida (2007), Energetic particle sounding of the magnetospheric cusp with ISEE-1, *Ann. Geophys.*, *25*, 1175–1182.
Zhang, H., T. A. Fritz, Q.-G. Zong, and P. W. Daly (2005), Stagnant exterior cusp region as viewed by energetic electrons and ions: A statistical study using Cluster Research with Adaptive Particle Imaging Detectors (RAPID) data, *J. Geophys. Res.*, *110*, A05211, doi:10.1029/2004JA010562.

E. Adamson and A. Otto, Geophysical Institute, University of Alaska Fairbanks, Fairbanks, AK 99775, USA.
K. Nykyri, Department of Physical Sciences, Embry-Riddle Aeronautical University, 600 S. Clyde Morris Blvd., Daytona Beach, FL 32114, USA. (nykyrik@erau.edu)
A. Tjulin, EISCAT Scientific Association, PO Box 812, SE-98128 Kiruna, Sweden.